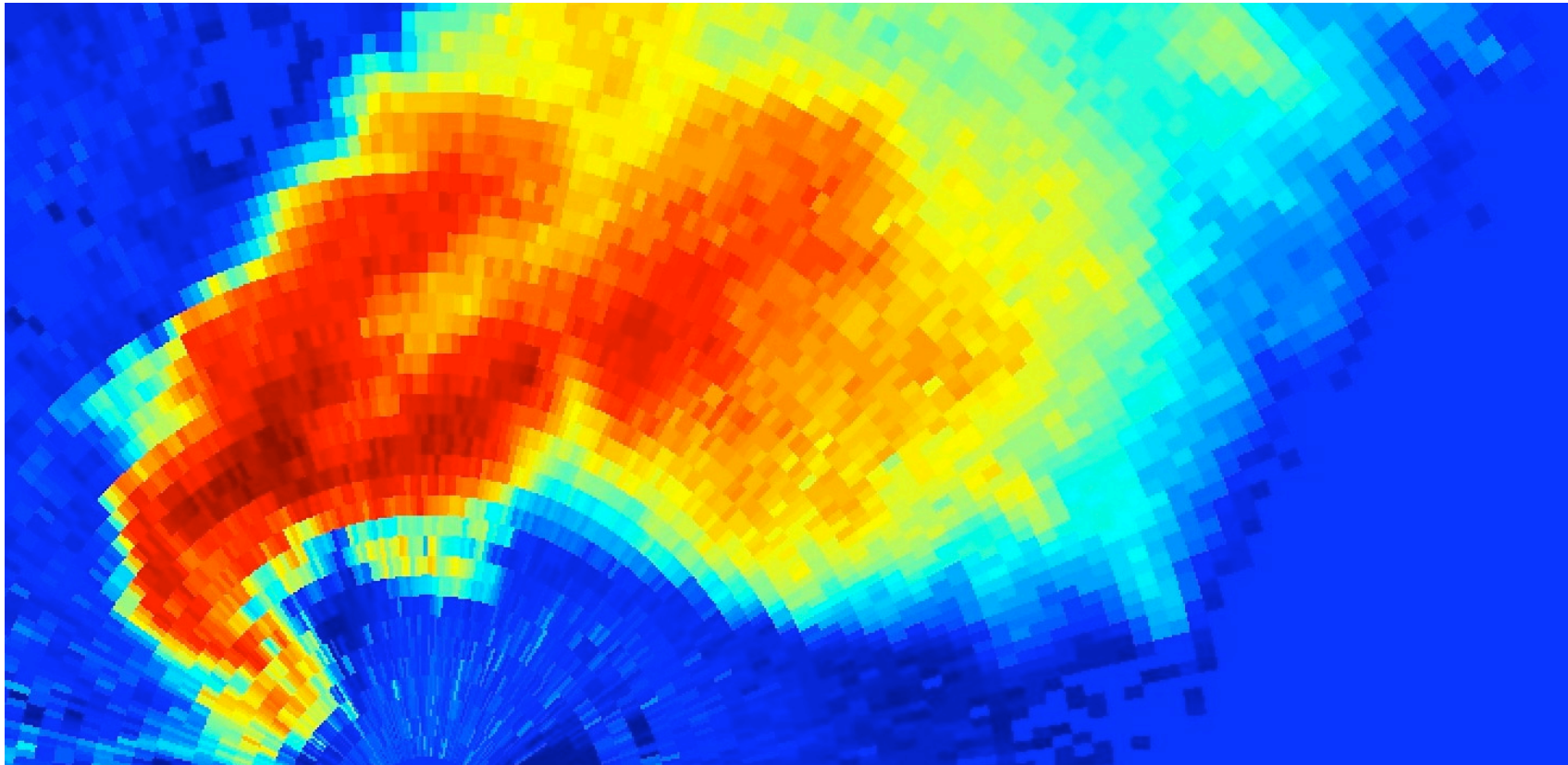# Techniques of dual-Doppler radar wind analysis: a review and new methodologies

[10 June 2010, Geophysical Colloquium, University of Hamburg]

by Alan Shapiro

*School of Meteorology, University of Oklahoma, Norman, Oklahoma, USA*

The Doppler effect

Waves (e.g., sound, radio, light) of a given frequency are emitted from a source, strike an object, and are reflected back toward source.

If the object is moving toward the source then the apparent frequency of the reflected wave <u>increases</u> over that of the transmitted wave.

The speed of the object can be estimated from this frequency shift!

Outgoing waves

Radar gun

Reflected waves (higher frequency)
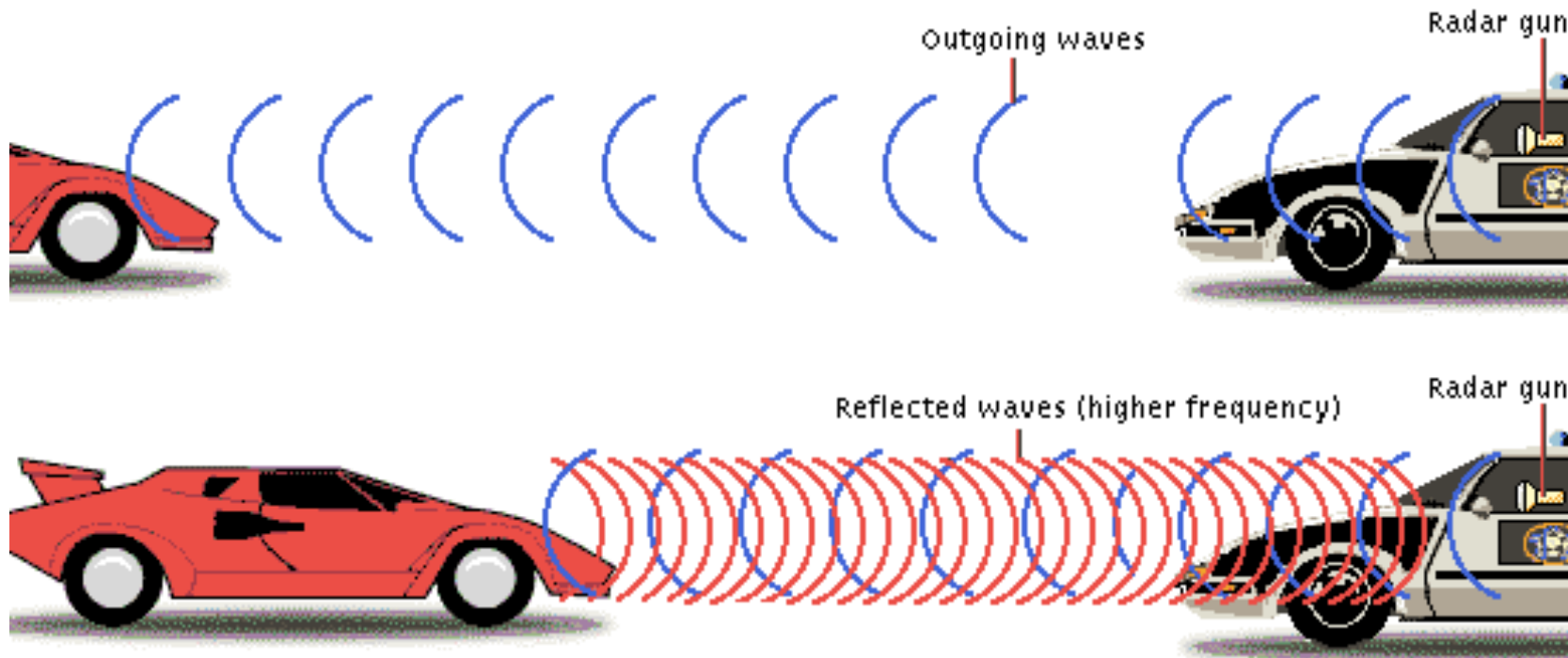
Radar gun

Use of Doppler frequency shift in speed estimates

- Astronomy (radiation emitted from planets, stars and galaxies)

- Law enforcement (radio waves from radar guns reflect off cars)

- Medicine (ultrasound waves bounce off blood cells)

- Meteorology (radio waves from radar bounce off hydrometeors)

4
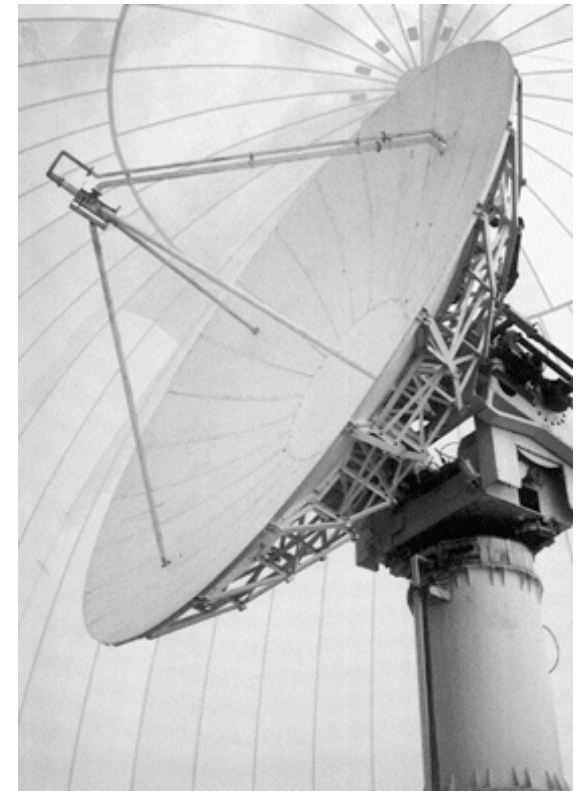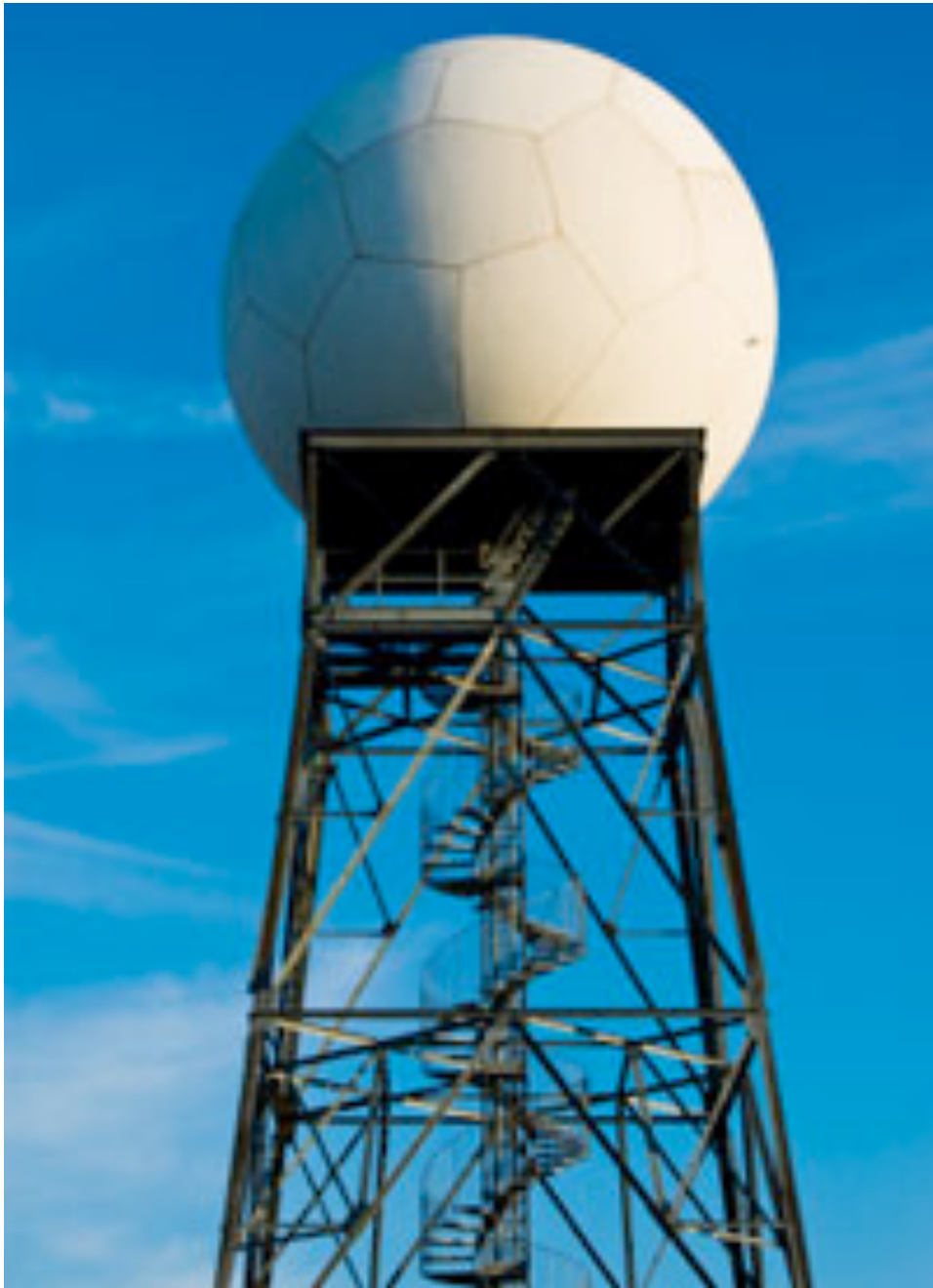
Doppler radar radial velocity component (v_r)
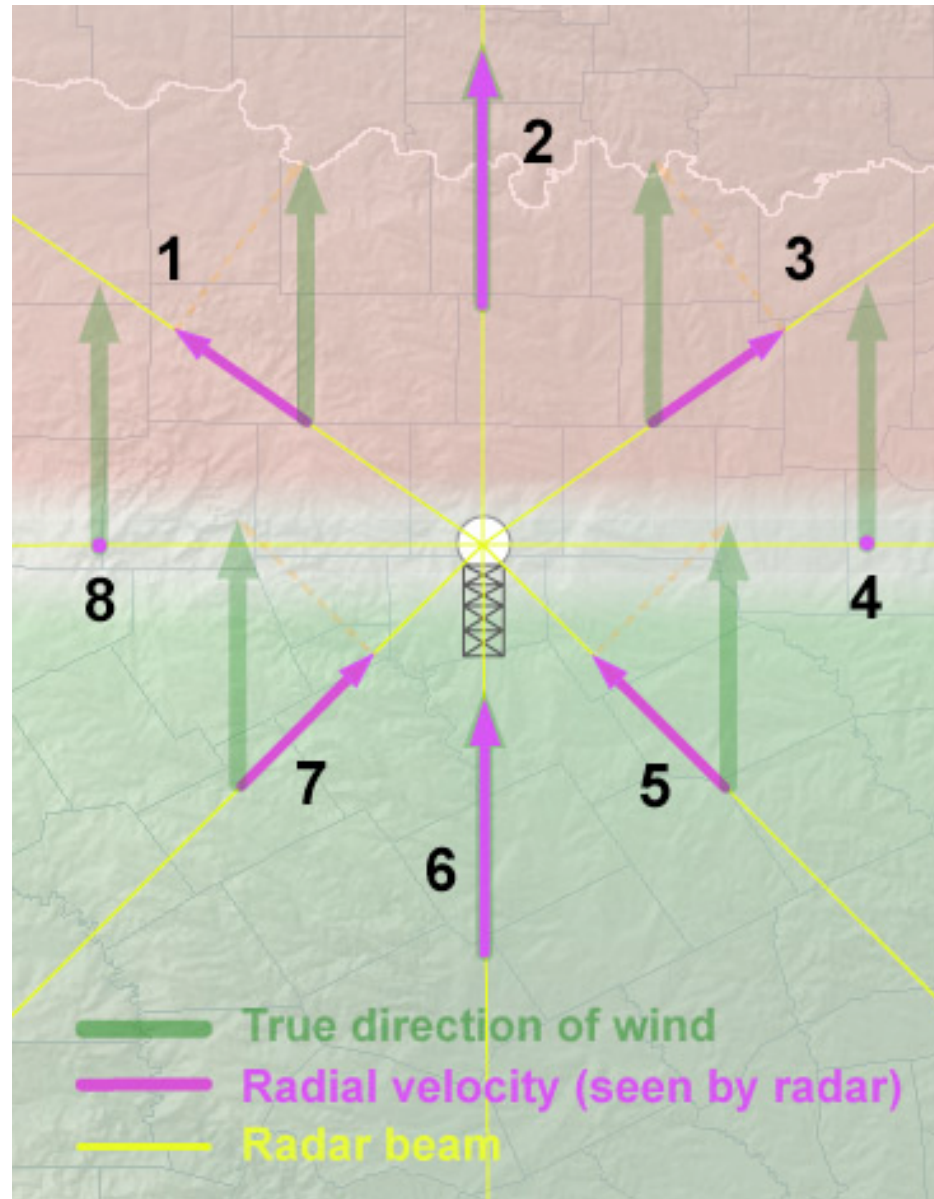
Radar reflectivity factor (*Z*)

Doppler radars also measure how much energy is reflected back. The **radar reflectivity factor *Z*** is a measure of the efficiency of a radar target (e.g. raindrop) in intercepting and returning radio energy.

Z varies strongly with drop diameter *D*:

$$Z = \int_0^\infty N(D) D^6 \, dD, \tag{1}$$

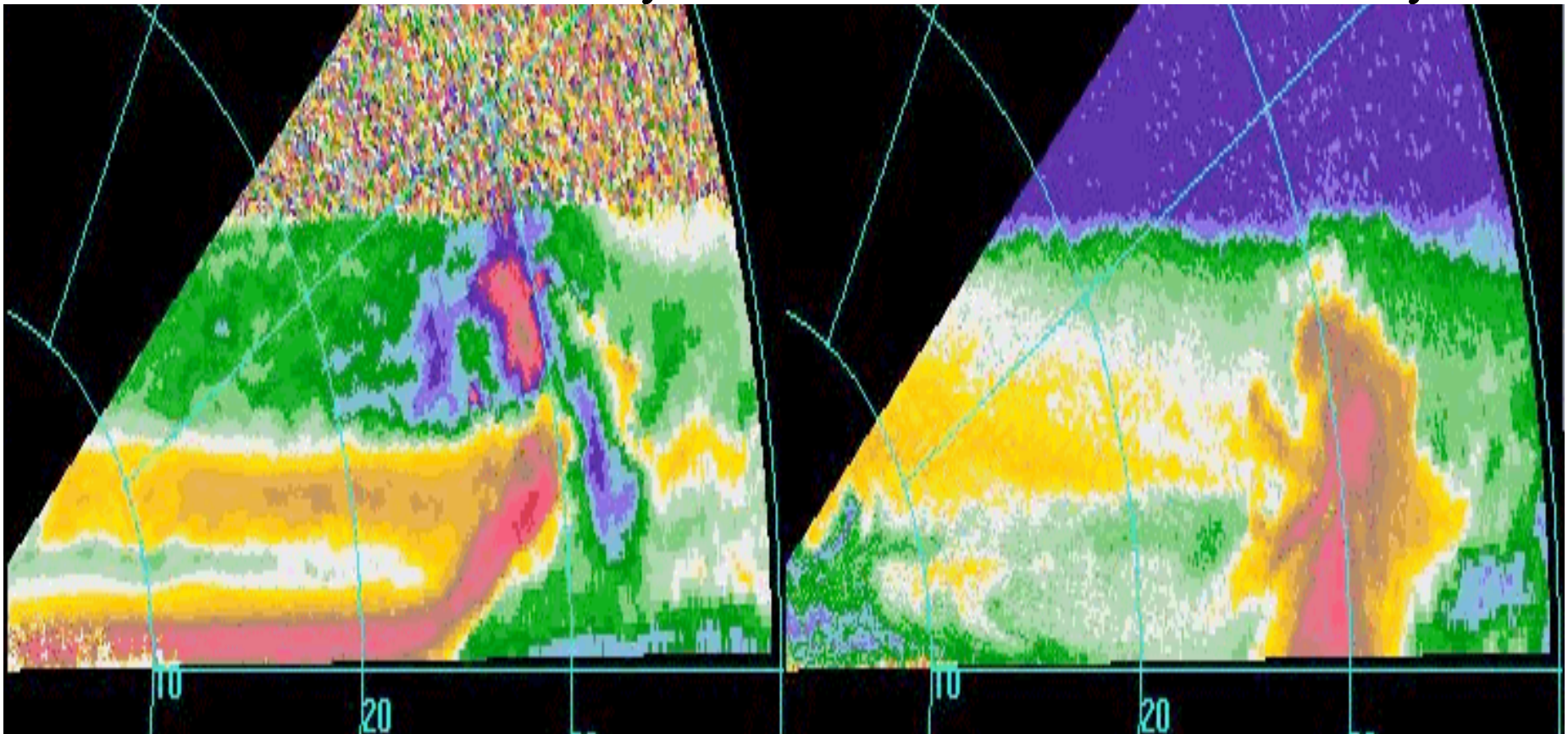where $N(D)$ is the number concentration of the raindrops.

The raindrop terminal velocity w_t can be estimated from *Z* by applying standard empirical relations such as $w_t = a D^b$, $N = N_0 \exp(-\Lambda D)$ in (1).
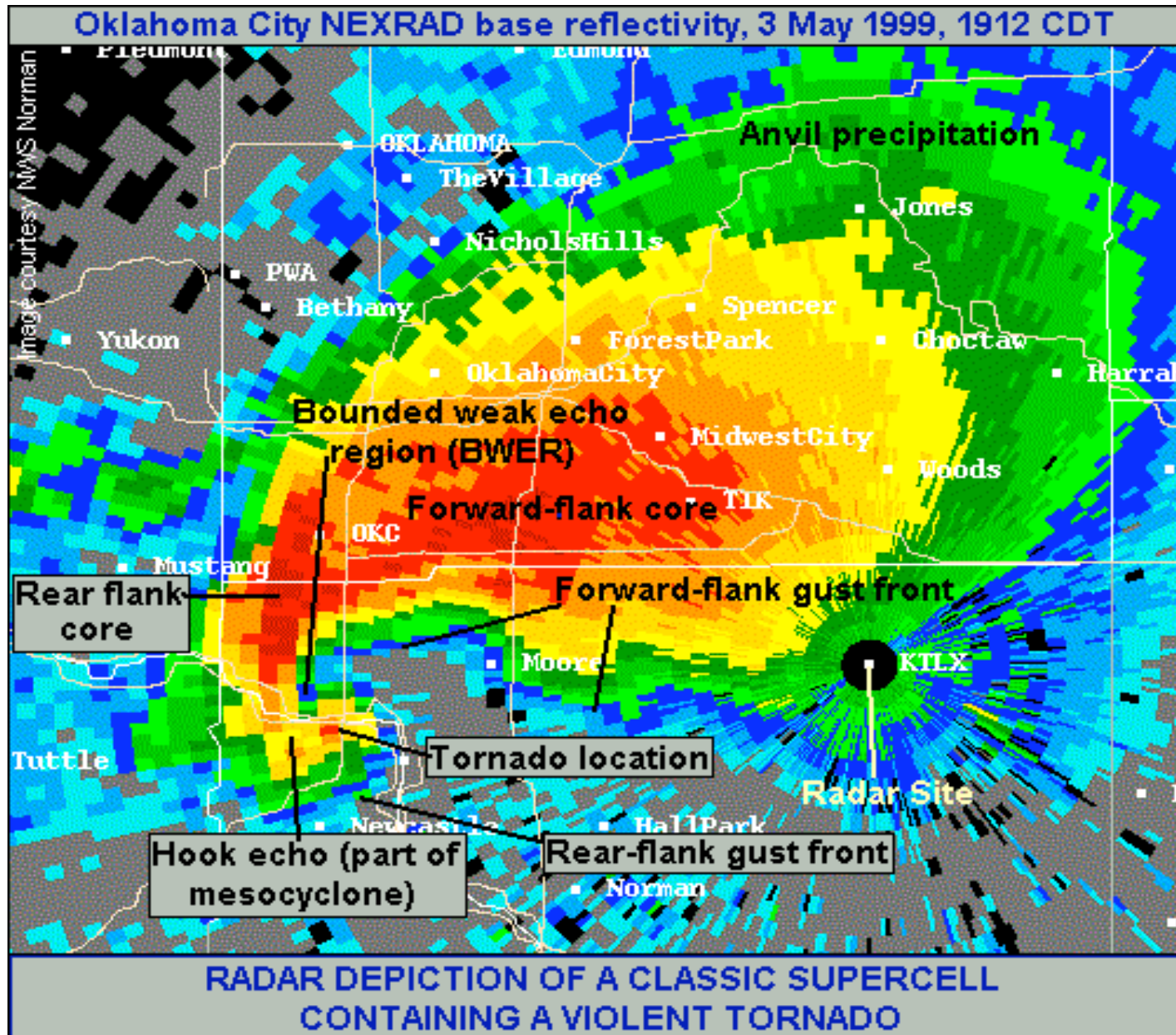
Examples of Doppler radar imagery

Vertical slice through a cold front

radial velocity   reflectivity

3 May 1999 tornadic supercell (reflectivity from a WSR-88D radar)

Oklahoma City NEXRAD base reflectivity, 3 May 1999, 1912 CDT

RADAR DEPICTION OF A CLASSIC SUPERCELL CONTAINING A VIOLENT TORNADO

10 May 2010 tornadic supercell (reflectivity from OU-PRIME)
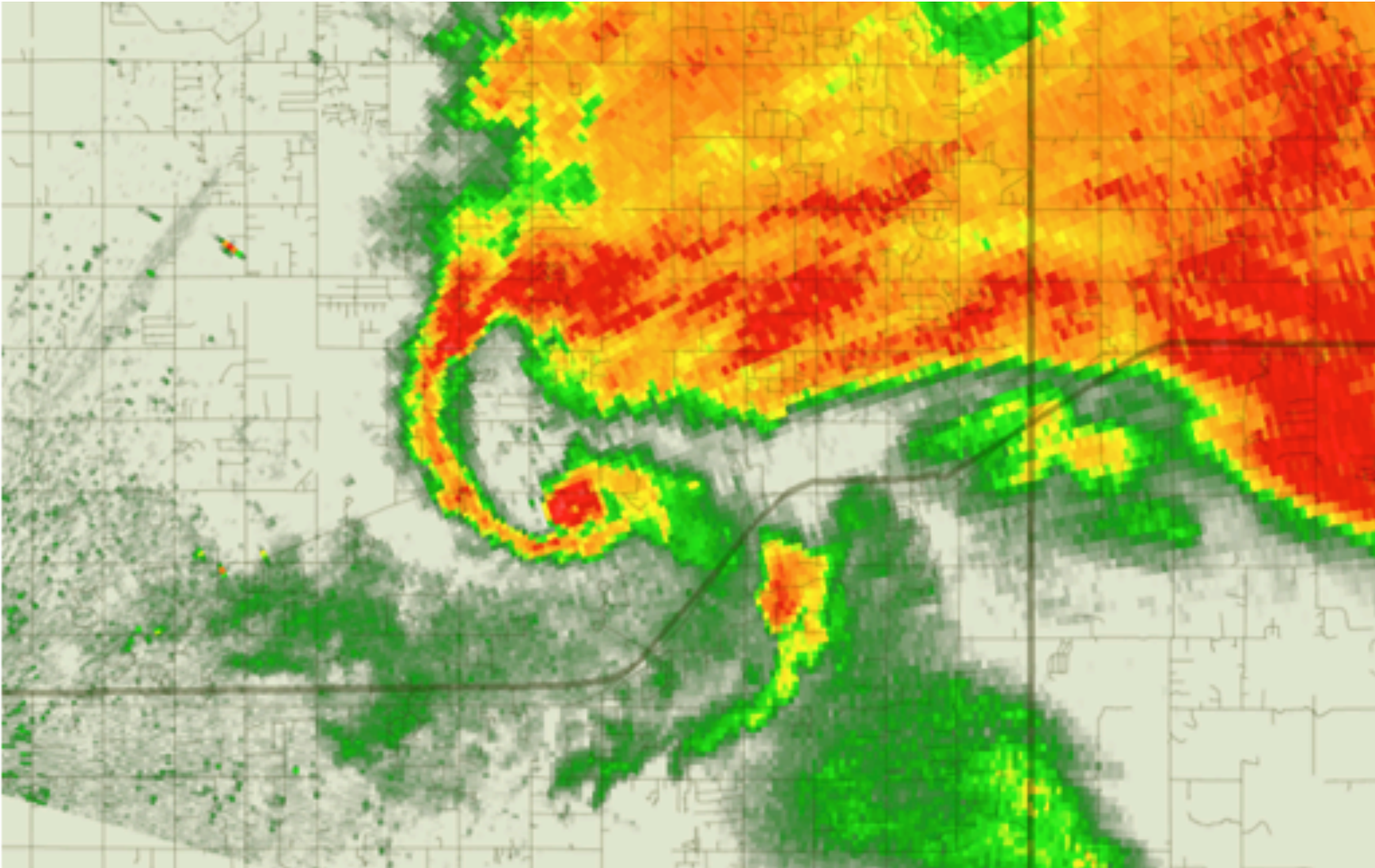
Doppler-on-Wheels reflectivity in a developing tornado
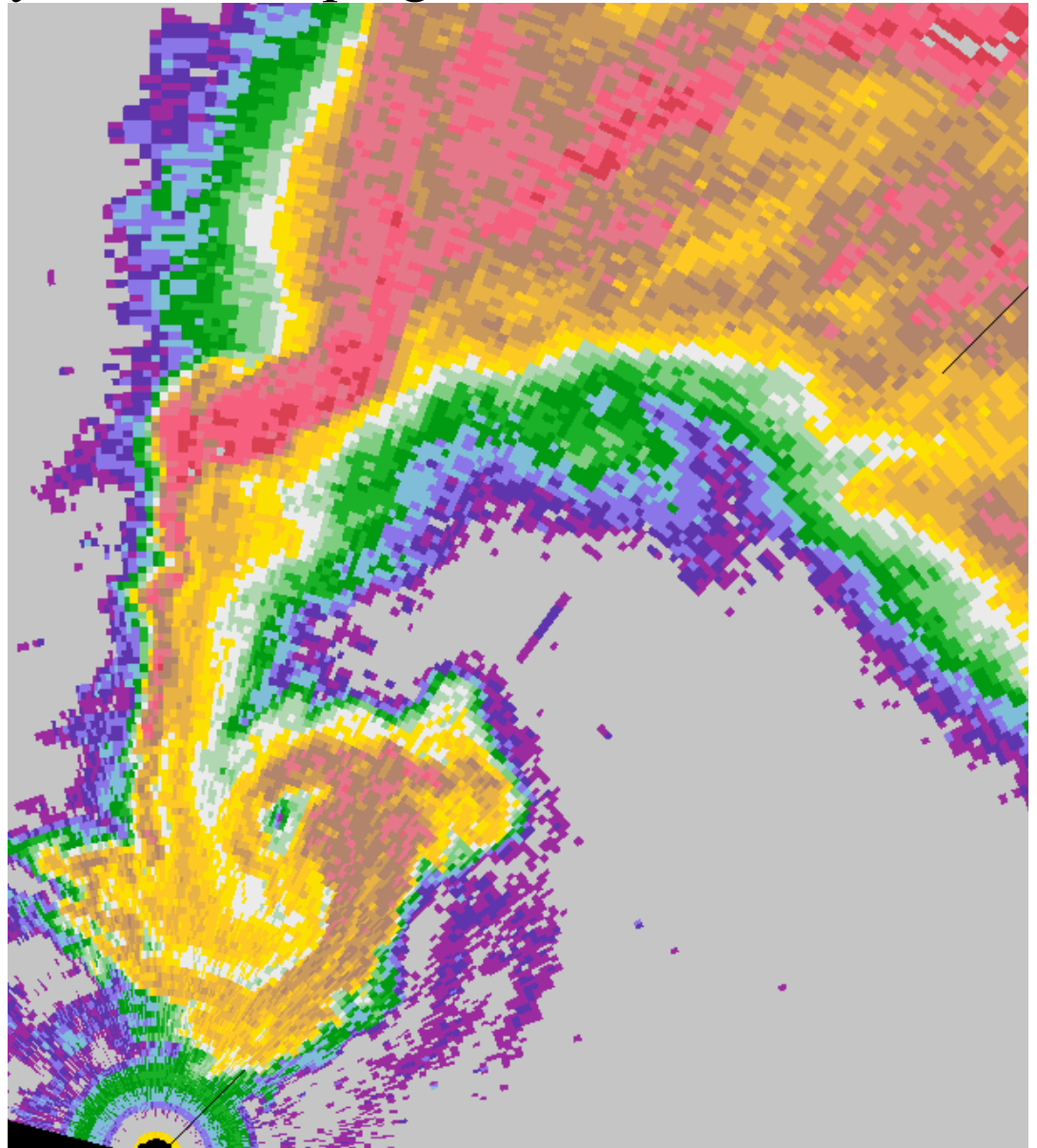
Another high-resolution Doppler-on-Wheels tornado

radial velocity   reflectivity
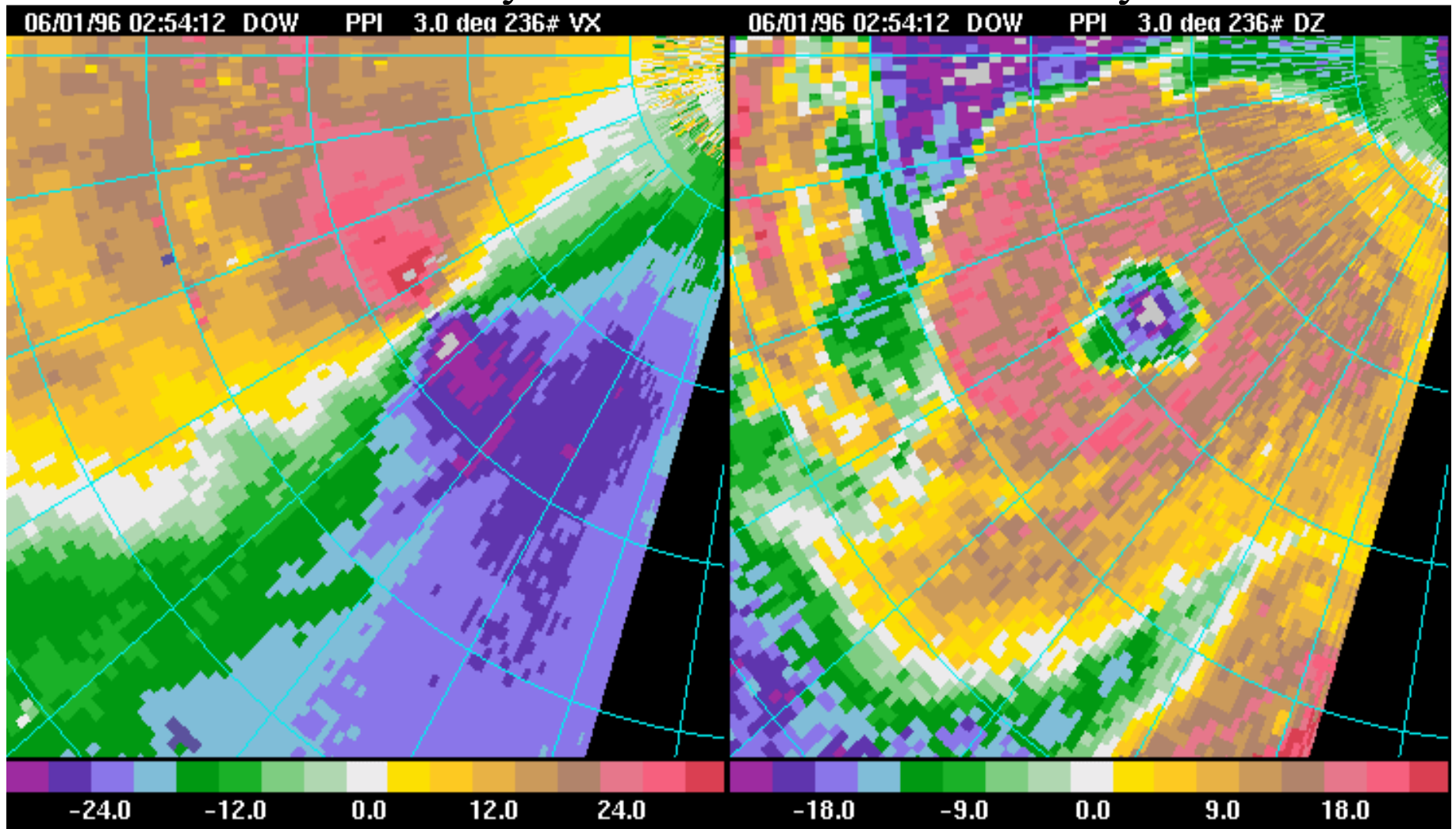
Dual-Doppler wind and thermodynamic analysis

Given one velocity component v_r (and Z) from two Doppler radars, we want to derive u, v, w and maybe p' and ρ' and maybe even q_r and q_i.

Step 1: Wind analysis. Combine data from two radars (look at storm from two angles) with mass conservation, $\nabla \cdot [\rho_0(z)\vec{u}] = 0$ to get u, v, w.

Step 2: Thermodynamic analysis (Gal-Chen 1978)

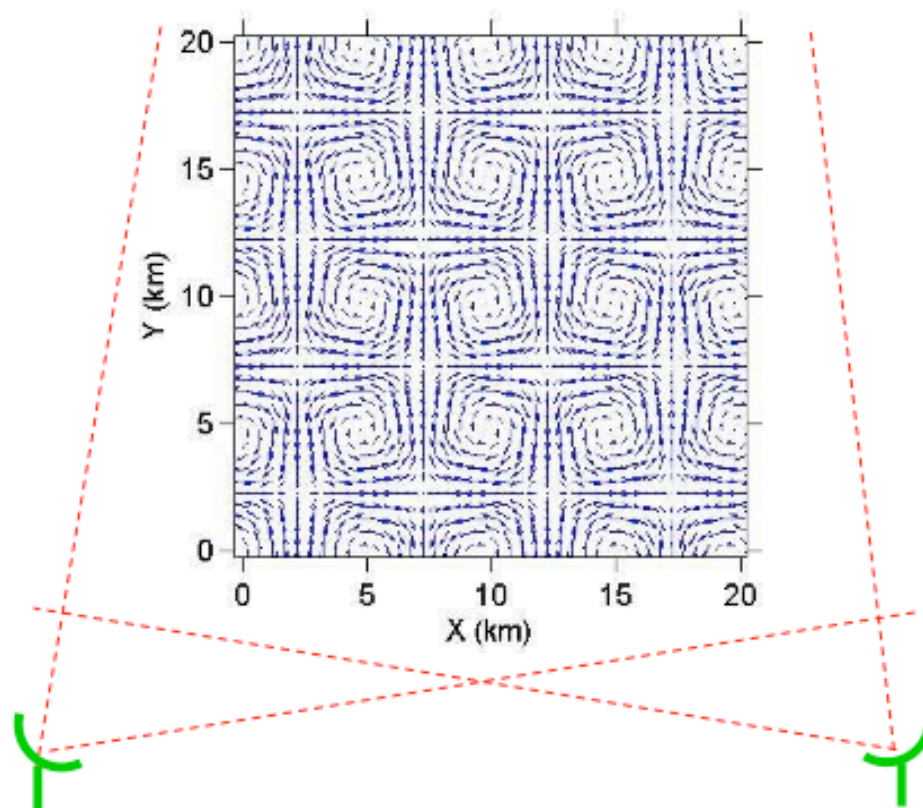Apply u, v, w from step 1 into the horizontal-motion Navier-Stokes equations,

$$\frac{\partial \vec{u}_h}{\partial t} + (\vec{u} \cdot \nabla)\vec{u}_h = -\frac{1}{\rho_0(z)}\nabla_h p' - f\hat{k} \times \vec{u}_h + \nu\nabla^2 \vec{u}_h. \qquad (2)$$

Taking $\nabla_h \cdot$ (2) yields a Poisson equation for p',

$$\nabla_h^2 p' = \text{known stuff}. \qquad (3)$$

Solve (3) for p' using Neumann boundary conditions inferred from (2).

Then, obtain ρ' from z-component Navier-Stokes equation,

$$\frac{\partial w}{\partial t} + (\vec{u} \cdot \nabla)w = -\frac{1}{\rho_0(z)}\frac{\partial p'}{\partial z} - g\frac{\rho'}{\rho_0(z)} + \nu\nabla^2 w.$$

Applications of dual-Doppler wind/thermodynamic analysis

Mesocyclones [Brandes 1984; Hane & Ray 1985; Dowell & Bluestein 1997; Wakimoto et al. 1998; Cai & Wakimoto 2001; Weygandt et al. 2002; Wurman et al. 2007]

Dual-Doppler analysis of tornadic supercell thunderstorms showed that

(i) an intense occlusion downdraft develops prior to tornadogenesis,

(ii) this downdraft is induced from a low-level vortex-induced vertical perturbation pressure gradient, and

(iii) this downdraft has a warm core.

Squall lines [Roux et al. 1984; Roux 1985, 1988; Lin et al. 1986, 1990; Hauser et al. 1988; Jorgensen et al. 1997; Liou et al. 2003]

Frontal rainbands [Parsons 1987; Roux et al. 1993]

Microbursts and downbursts (Kessinger et al. 1988; Parsons & Kropfli 1990)

Dual-Doppler analysis of a tornadic supercell (Wurman et al. 2007)
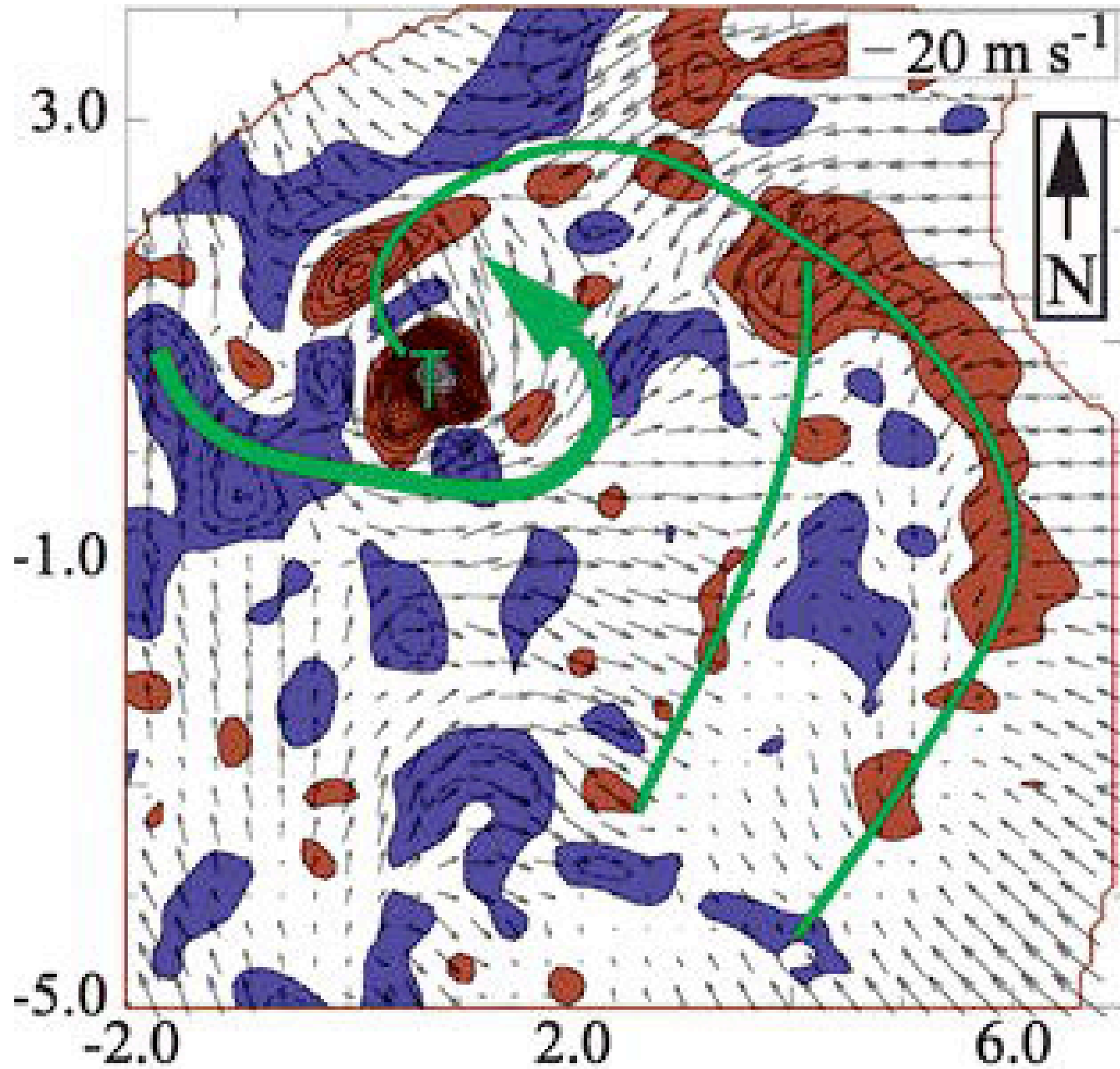
Exact theory for dual-Doppler wind analysis

Armijo (1969) derived the solution for a 3D velocity field $\vec{u}$ for which

(i) radial components of $\vec{u}$ agree with radial wind observations,

$$\vec{u} \cdot \hat{r}_1 = v_{r1}, \tag{4}$$

$$\vec{u} \cdot \hat{r}_2 = v_{r2}, \tag{5}$$

(ii) anelastic mass conservation equation is satisfied,

$$\nabla \cdot [\rho_0(z)\vec{u}] = 0, \tag{6}$$

(iii) impermeability condition is satisfied ($w = 0$ at ground level).

The u, v, w fields satisfy (4), (5), (6). Eliminating u and v in favor of w yields a 1st order partial differential equation for w. Get the exact analytical solution by integrating a forcing term along characteristics.

Coplane coordinate system

The characteristics in the Armijo theory are circles in a cylindrical coordinate system whose central axis connects the radars (baseline). To get w at any point (**A**), integrate the forcing term (data) along the circle passing through **A**. Start at the ground (**B**) where $w = 0$.

Well-posedness condition: a unique solution for w exists at **A** if there are data at all points from **A** to **B**. **No solution exists if data are missing anywhere between A and B.**
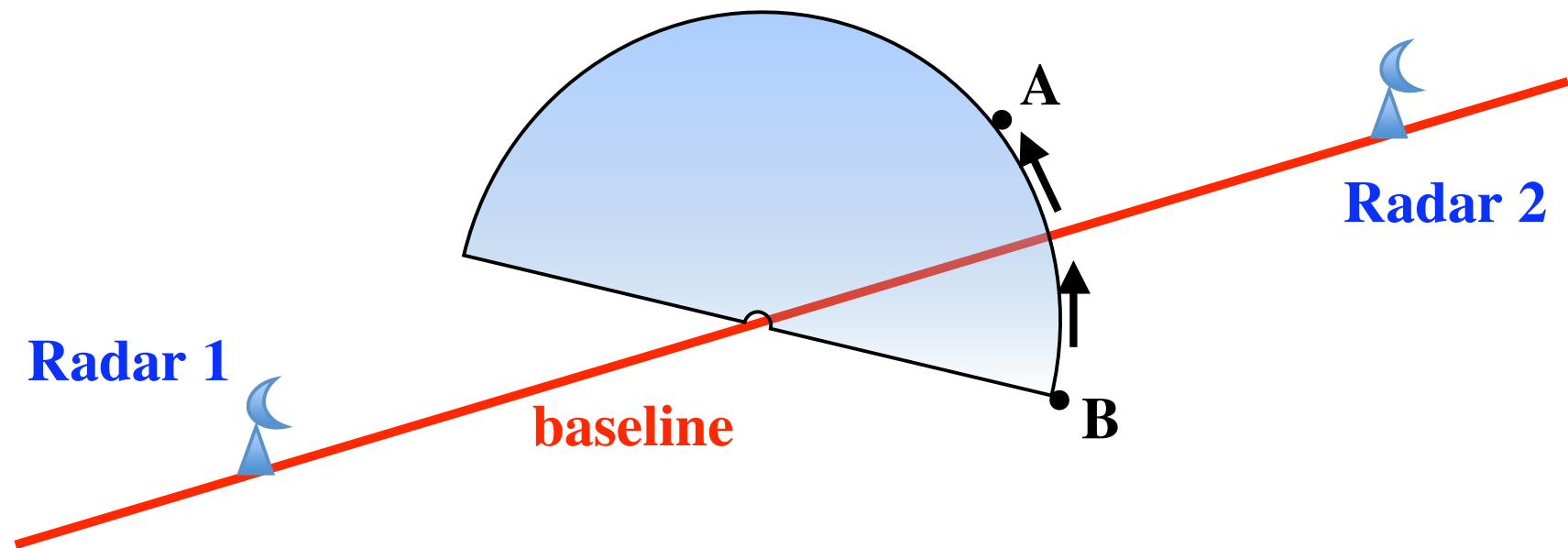
A Cartesian form of dual-Doppler wind analysis

Some investigators bypass Armijo's direct procedure, and solve (4), (5), (6) iteratively in a Cartesian coordinate system [Brandes 1977; Ray et al. 1980; Hildebrand & Mueller 1985; Dowell & Bluestein 1997]
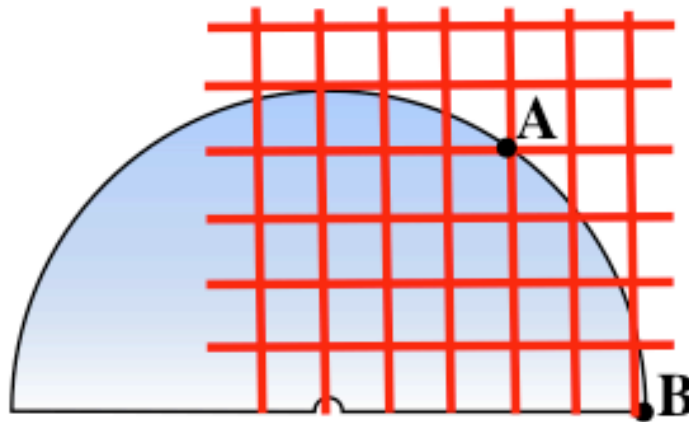
The iterative Cartesian analysis does not always converge. Dowell and Shapiro (2003) derived a stability condition that showed that Armijo's "well-posedness" condition was relevant even in Cartesian coordinates.

Even in cases where the analysis is well posed (either Armijo's Coplane analysis or the iterative Cartesian analysis), dual-Doppler analyses are still subject to a number of practical difficulties.

Ongoing challenges with dual-Doppler wind analysis: problems and some (partial) solutions

Problem 1: Non-simultaneous data collection can result in phase (location) errors in key features such as gust fronts and vortices.

Solution: Use "advection correction." Invoke the frozen-turbulence hypothesis to shift data from both radars to a common analysis time.

t = 0 min   t = 5 min

19
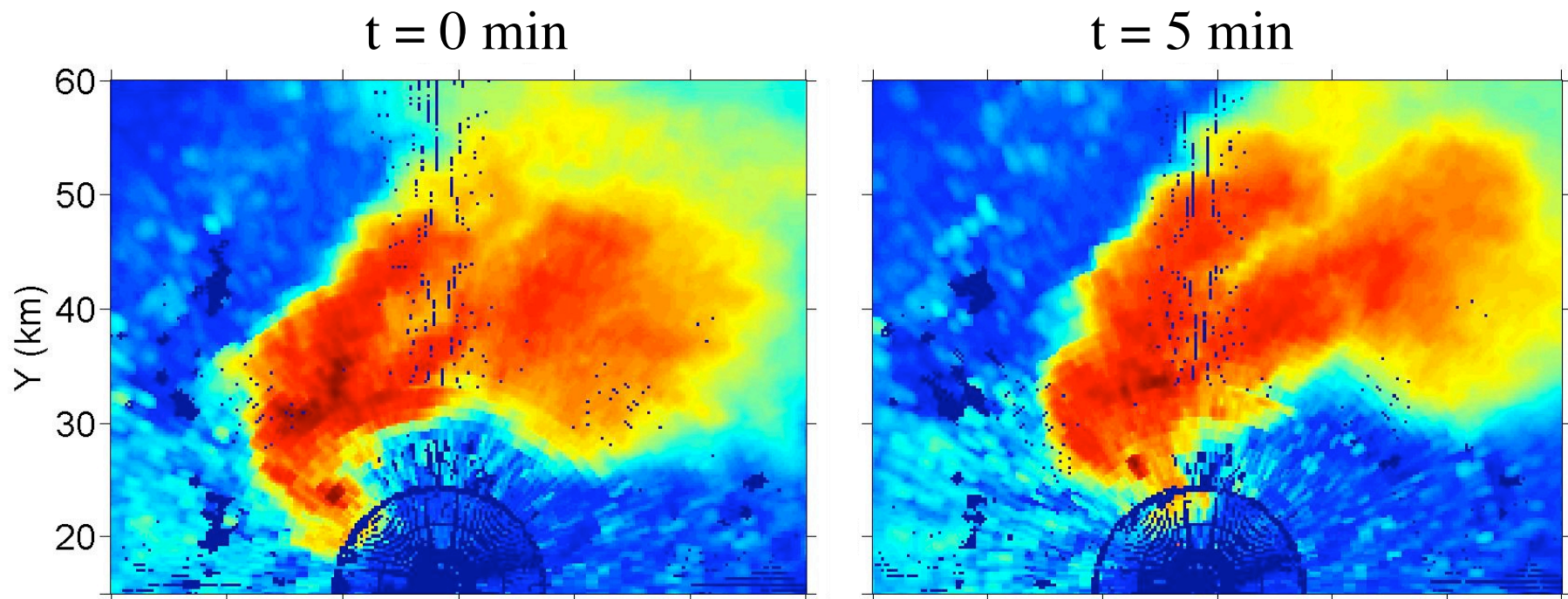
Frozen-turbulence hypothesis

Frozen-turbulence hypothesis: patterns translate (shift) without change in shape or intensity. In the case of the reflectivity field Z, this implies:

$$\frac{\partial Z}{\partial t} + U\frac{\partial Z}{\partial x} + V\frac{\partial Z}{\partial y} = 0, \tag{7}$$

where U, V are pattern-translation components (<u>not</u> wind velocity components).

Many methods are available to estimate U, V (e.g., Gal Chen 1982), however these generally treat U and V as constants over the whole grid.

We will consider a procedure to derive/use spatially-variable U, V fields in advection correction.

Problem 2: Biases in the divergence can quickly accumulate in the integration process and yield catastrophic errors in *w*.

Solution: Use radial wind data and mass conservation equation $\nabla \cdot [\rho_0(z)\vec{u}] = 0$ as weak constraints (least squares error) in a variational procedure, e.g. 3DVAR or 4DVAR.

We will look at an example of this later.

Problem 3: Missing low-level data due to earth curvature, ground clutter, or non-zero elevation angle of lowest sweep.

$\theta = 15°$

$\theta = 0°$
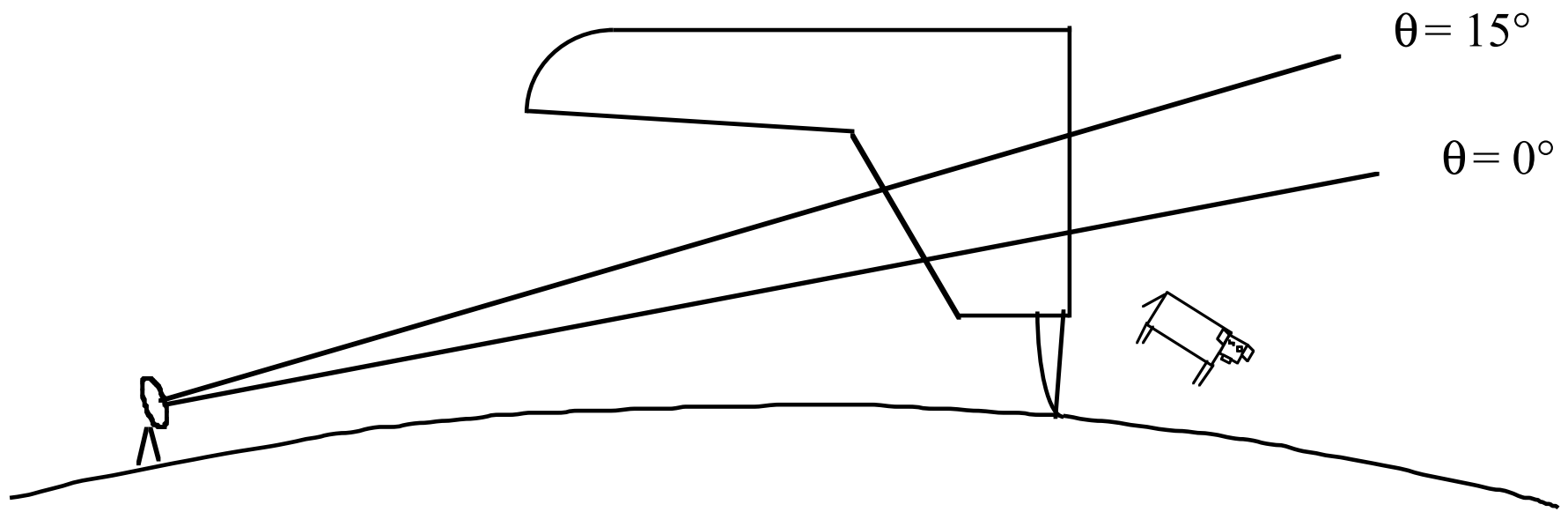
Solution: Extrapolate data from the lowest sweep down to the ground.

Alternatively, use another constraint, e.g. a vorticity equation. **We will also look at this later.**

Spatially variable advection correction

We seek $U(x, y)$, $V(x, y)$ and reflectivity $Z(x, y, t)$ fields on horizontal or constant elevation angle surfaces that **minimize the cost function:**

$$J \equiv \iiint \left[\alpha \left(\frac{\partial Z}{\partial t} + U \frac{\partial Z}{\partial x} + V \frac{\partial Z}{\partial y} \right)^2 + \beta \left| \nabla_h U \right|^2 + \beta \left| \nabla_h V \right|^2 \right] dx \, dy \, dt, \quad (8)$$

with Z imposed at two effective data times, $t = 0$ and $t = T$.

β is a smoothness coefficient; α is a data coverage function ($= 0$ or 1) that satisfies $\frac{\partial \alpha}{\partial t} + U \frac{\partial \alpha}{\partial x} + V \frac{\partial \alpha}{\partial y} = 0$.

A similar J underpins some single-Doppler velocity retrievals (Laroche & Zawadzki 1995; Liou & Luo 2001) and some precipitation nowcasting algorithms (Germann & Zawadzki 2002).

Euler-Lagrange equations

Two elliptic equations,

$$\beta T \frac{\partial^2 U}{\partial x^2} + \beta T \frac{\partial^2 U}{\partial y^2} = \int \alpha \frac{\partial Z}{\partial t} \frac{\partial Z}{\partial x} \, dt + U \int \alpha \left(\frac{\partial Z}{\partial x} \right)^2 dt + V \int \alpha \frac{\partial Z}{\partial x} \frac{\partial Z}{\partial y} \, dt, \quad (9)$$
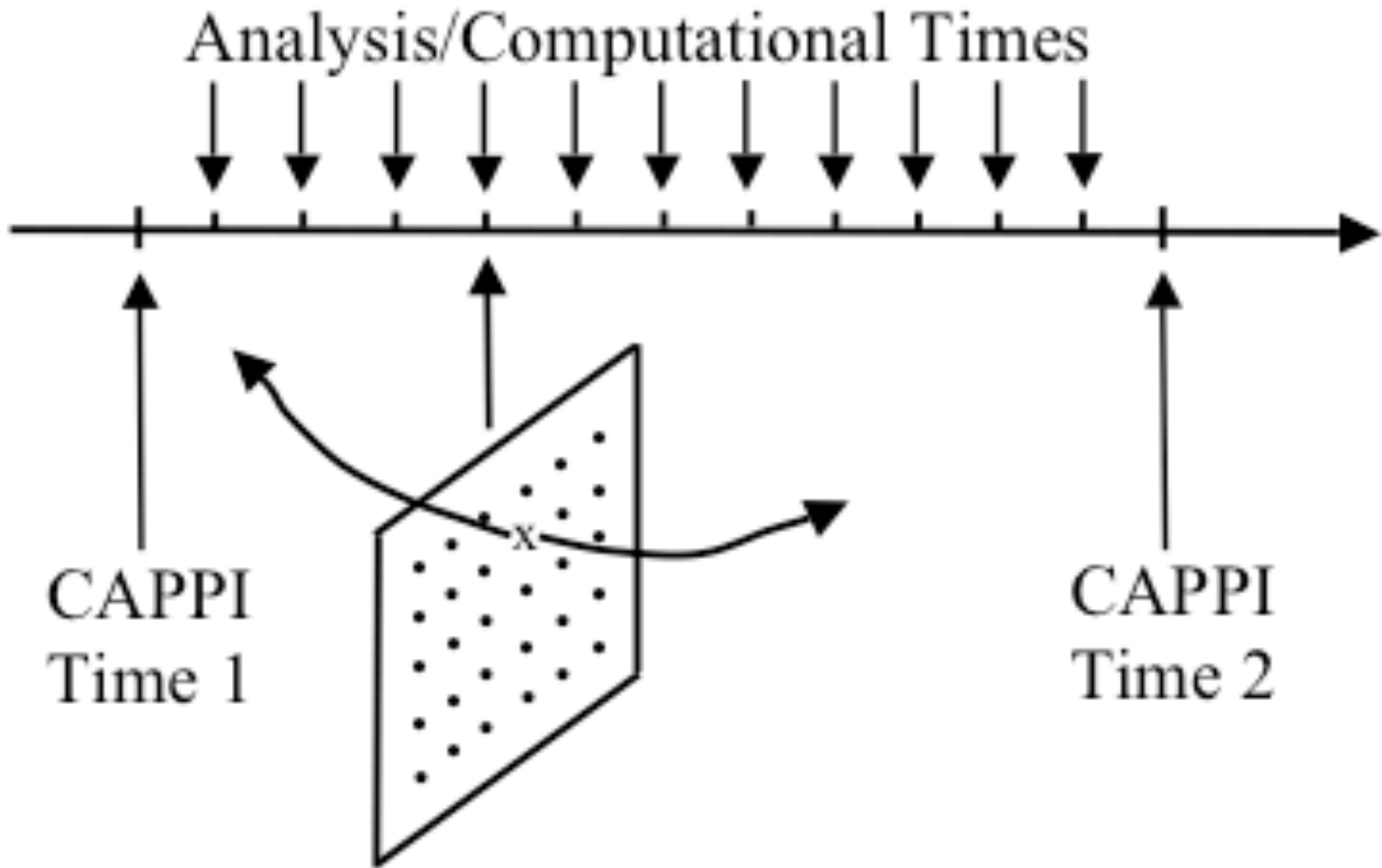
$$\beta T \frac{\partial^2 V}{\partial x^2} + \beta T \frac{\partial^2 V}{\partial y^2} = \int \alpha \frac{\partial Z}{\partial t} \frac{\partial Z}{\partial y} \, dt + U \int \alpha \frac{\partial Z}{\partial x} \frac{\partial Z}{\partial y} \, dt + V \int \alpha \left(\frac{\partial Z}{\partial y} \right)^2 dt, \quad (10)$$

and one parabolic equation,

$$\alpha \left(\frac{\partial}{\partial t} + U \frac{\partial}{\partial x} + V \frac{\partial}{\partial y} \right)^2 Z + \alpha \left(\frac{\partial U}{\partial x} + \frac{\partial V}{\partial y} \right) \left(\frac{\partial Z}{\partial t} + U \frac{\partial Z}{\partial x} + V \frac{\partial Z}{\partial y} \right)$$

$$+ \left(\frac{\partial \alpha}{\partial t} + U \frac{\partial \alpha}{\partial x} + V \frac{\partial \alpha}{\partial y} \right) \left(\frac{\partial Z}{\partial t} + U \frac{\partial Z}{\partial x} + V \frac{\partial Z}{\partial y} \right) = 0. \quad (11)$$

The characteristics of (11) are solutions of $Dx/Dt = U$, $Dy/Dt = V$, which are the equations for trajectories. Can solve (11) analytically.

Analysis grid

Analysis/Computational Times

CAPPI
Time 1

CAPPI
Time 2

x

Combined analytical/numerical solution

Iterate between these steps:

Step 1: Solve the elliptic equations for U and V by relaxation.

Step 2: Calculate forward and backward trajectories running through all analysis points at a set of computational times.

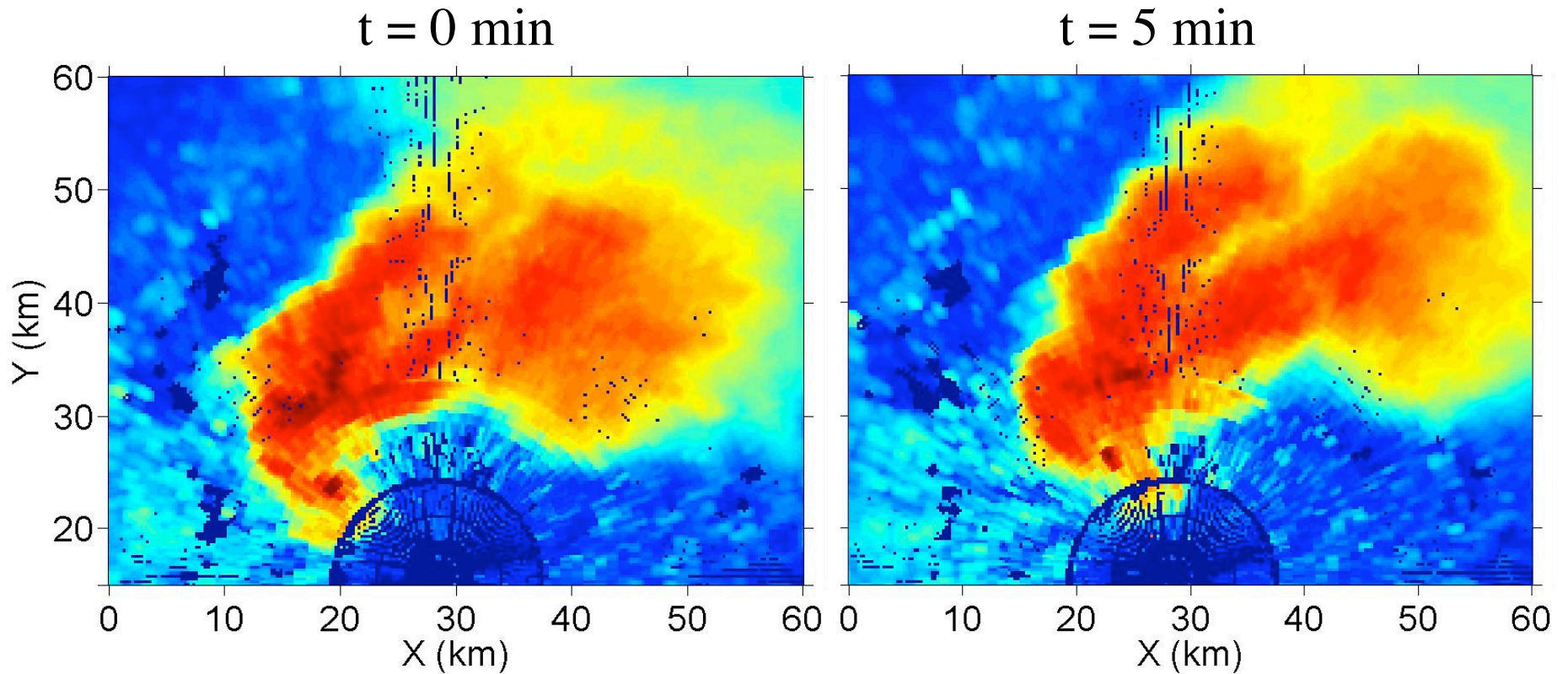Step 3: Interpolate Z data to the end-points of each trajectory.

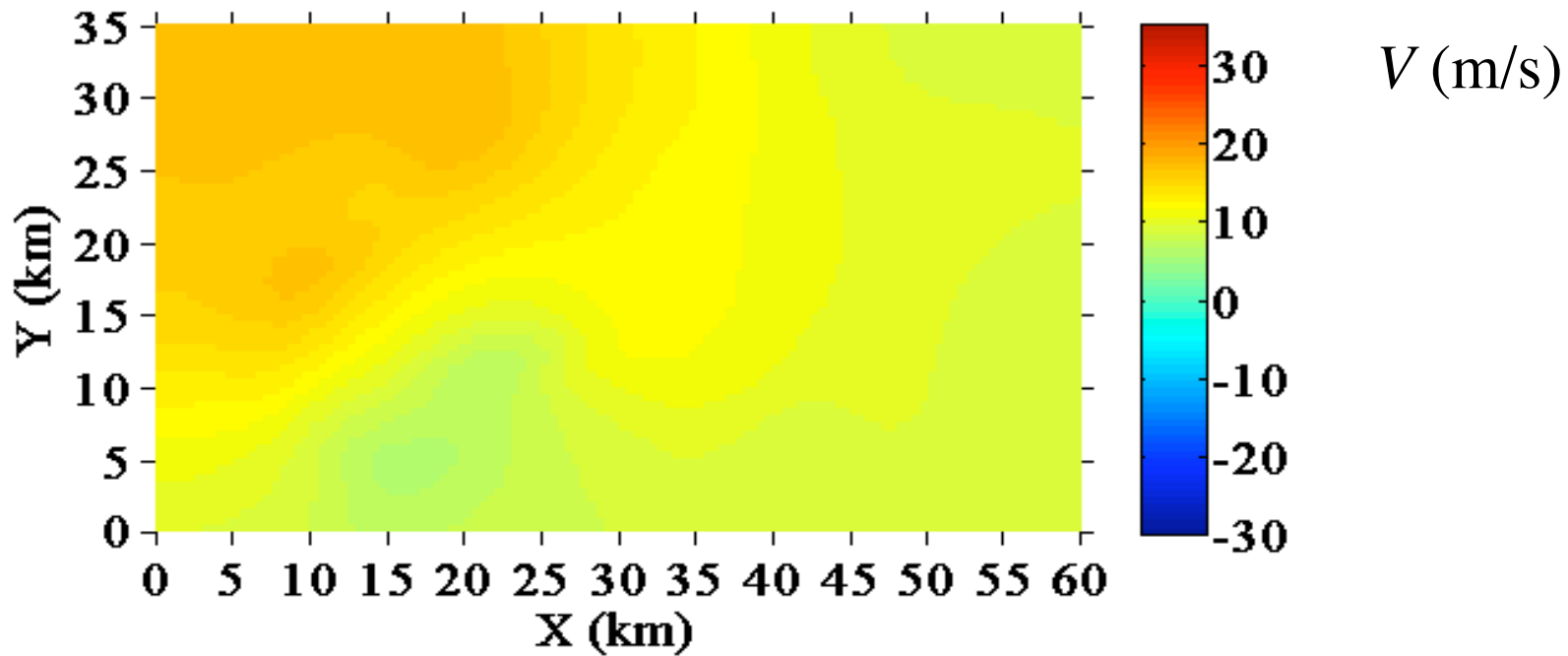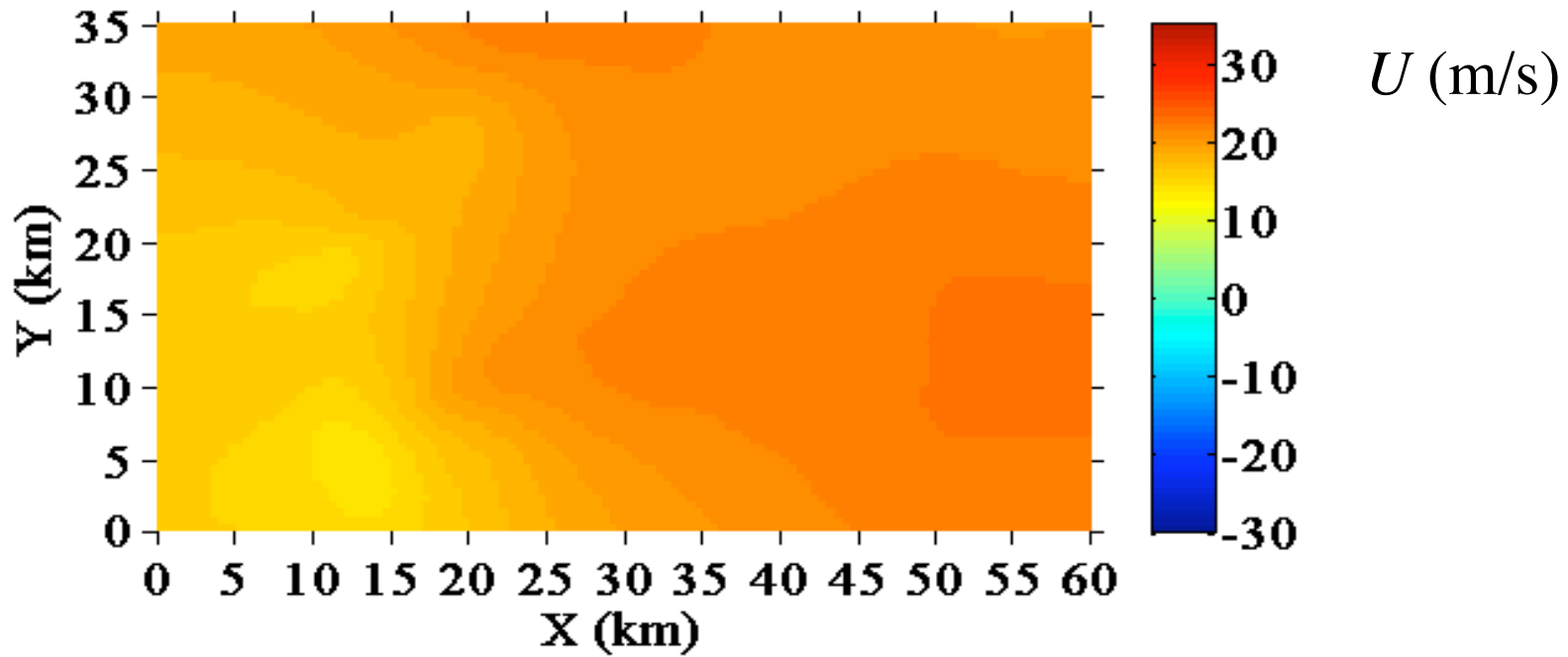Step 4: Update Z by evaluating the analytical solution of the parabolic equation for Z.

$$Z(t) = Z(t_0) + \left[Z(t_0 + T) - Z(t_0) \right] \frac{I(t)}{I(t_0 + T)}, \qquad (12)$$

$$\text{where} \quad I(t) \equiv \int_{t_0}^{t} \exp\left[\int_{t_0}^{t'} \left(\partial U/\partial x + \partial V/\partial y \right) dt'' \right] dt'.$$

Test case: Oklahoma supercell storm, 8 May 2003

Input data: Two scans of WSR-88D radar reflectivity (KTLX radar)

U (m/s)

V (m/s)

28

Quantitative verification using a TDWR radar

Tests with a second radar (TDWR) gave similar results but were better suited for quantitative verification: data available every ~1 min, so could compare advection-corrected *Z* with true *Z* at an intermediate time. **RMS error in spatially variable *U*, *V* experiment (~ 4.5 dBZ) is less than RMS errors obtained in any constant *U*, *V* experiments:**
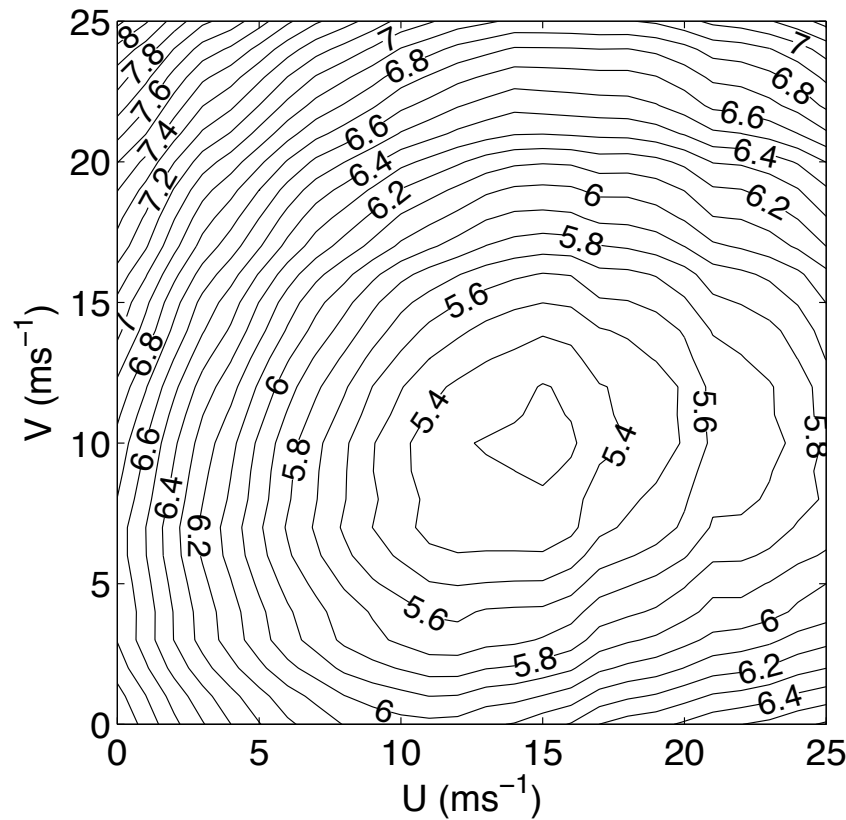
Use of a mesoscale vertical vorticity equation in dual-Doppler wind analysis